MicroRiYo : An observing system for deep repeated profiles of kinetic energy dissipation rates from shear-microstructure turbulence along a mooring line

Ferron, B.,[a] S. Leizour,[a] M. Hamon,[a] O. Peden[a]

[a] *Univ. Brest, CNRS, IFREMER, IRD, Laboratoire d'Océanographie Physique et Spatiale, IUEM, Brest, France*

Corresponding author: B. Ferron, bferron@ifremer.fr

File generated with AMS Word template 2.0

Early Online Release: This preliminary version has been accepted for publication in *Journal of Atmospheric and Oceanic Technology*, may be fully cited, and has been assigned DOI 10.1175/JTECH-D-24-0009.1. The final typeset copyedited article will replace the EOR at the above DOI when it is published.

ABSTRACT

A new observing system that provides deep repeated profiles of the oceanic kinetic energy dissipation rate and small-scale mixing is presented. The system is designed to provide 300 dissipation rate profiles using a vehicle that cycles along a mooring line from the sub-surface down to a maximum depth of 4000 m. The system was tested for two weeks between 630 and 1700 m during a cruise that took place on the Lucky Strike segment of the Mid-Atlantic Ridge. The vehicle collected 35 profiles at a mean downcast velocity of 0.63 m s^{-1}. To quantify the quality of the measurements, profiles from the mooring are compared with nearby profiles from an autonomous microstructure free-falling instrument. The dissipation rate noise level varies between O(10^{-10}) and O(10^{-9}) W kg^{-1}. This noise level is low enough to detect turbulent patches at depth. The largest dissipation rate measured at this site was O(10^{-7}) W kg^{-1}.

SIGNIFICANCE STATEMENT

Understanding how the ocean dissipates the energy it receives from astronomical and atmospheric forcing (tides, heat, freshwater, wind) is a key element of the ocean dynamics. Here, we present a new observing system that allows repeated measurements of the dissipation of kinetic energy in the ocean from the subsurface down to 4000 m at a given geographical point. Three hundred profiles can be measured, providing insights into the dynamics responsible for energy dissipation and tracer mixing. This observing system is particularly suited to the deep open ocean, where such observations remain scarce.

1. Introduction

Direct observations of ocean turbulence using the microstructure sensors have become more common in the last two decades with the advent of microstructure instruments on the market (Prandke et al. 2000; Wolk et al. 2002; Fer et al. 2014). These observations still remain far less frequent than the widely used Conductivity-Temperature-Depth (CTD) package. The recent multiplication of ocean microstructure observations has helped to better assess the role of diapycnal mixing and dissipation of kinetic energy in different dynamical environments. However, deep observations of turbulence remain challenging for several reasons, including pressure effects and the presence of topography. Nevertheless, it is

Accepted for publication in *Journal of Atmospheric and Oceanic Technology.* DOI 10.1175/JTECH-D-24-0009.1.

recognized that deep turbulence, which is often associated with topographic features, is a key component of the oceanic machinery (e.g. de Lavergne et al. 2016, 2020; Polzin and McDougall, 2022). Observing and identifying the dynamics of the energy sources that feed this deep turbulence remains necessary and requires adequate observing systems. Here, we report on the development of a mooring capable of providing 300 repeated vertical profiles of microstructure shear down to 4000 m depth.

2. MicroRiYo

a. Overview

The MicroRiYo (MRY) mooring concept was originally inspired by a CTD mooring (Budéus et al. 2005). It consists of a vehicle moving quasi freely along a mooring line (Fig. 1). The vehicle carries a MicroRider 6000 and a CTD (www.rockland.com). It has a positive buoyancy and waits at the top of the mooring line, below a weight dispenser. The weight dispenser releases a weight at a prescribed frequency into a basket located at the top of the vehicle. This weight provides a negative buoyancy to the vehicle, which then slides down the mooring line to a stopper. Measurements are taken only during the downcast, as microstructure sensors are located at the bottom of the vehicle. When the vehicle hits the stopper, it drops its weight, which falls into a collector located below the stopper. The vehicle regains its positive buoyancy and begins its ascent until it reaches the weight dispenser, where it waits for the next release. The MicroRider is equipped with two Rockland Scientific fast thermistors (FP-07), one Sea-bird Electronics (SBE) microconductivity sensor (SBE-7), and two Rockland Scientific velocity shear probes (SPM-38). The microstructure sensors are sampled at 512 Hz.

b. Weight dispenser

The weight dispenser consists of a circular stainless steel frame with a diameter of 80 cm and a height of 140 cm (Fig. 2). Four pipes, each 8cm in diameter, are wound helically around this frame, giving a total diameter of 102 cm. Each pipe can hold 100 weights. Each

Accepted for publication in *Journal of Atmospheric and Oceanic Technology.* DOI 10.1175/JTECH-D-24-0009.1.

weight is made of lead with a diameter of 6.3 cm for a mass of ~1.3 kg in seawater. At the base of the frame, the weights are transferred to the vehicle by means of a disk (diameter 60 cm) rotating over a fixed square plate (size 60 cm), both 7 cm thick. The disk and the plate, made of polyoxymethylene (or polyacetal, a thermoplastic material), are separated by a gap of 0.4 cm with 8 stainless steel balls evenly distributed to facilitate the rotation of the disk on the plate. Initially, the weights stored in the pipes rest on the rotating disk. When the disk starts rotating, four weights fall simultaneously into the four holes (diameter 6.5 cm) evenly drilled in the rotating disk and sit on the plate. The plate is also drilled with 4 holes (diameter 6.5 cm) unevenly distributed (see inset on Fig. 2 for a top view of the rotating disk and plate). Every weight release period, the disk starts rotating by ~22.5° until one of the four weights falls into one of the holes of the plate. The released weight then falls into a funnel below the plate and is channeled by a soft pipe to the vehicle basket located 50 cm below the dispenser (Fig. 2). A full 360° rotation of the disk releases 16 weights. Only 18.75 full rotations are required to release 300 weights. The funnel system adds 50 cm to the height of the dispenser. As an example, the inset in Fig. 2 shows the state of the rotating disk when the four weights have just been loaded. When the disk then rotates 22.5° from this position, weight #1 falls into the funnel, passing through hole #A of the square plate. On the next rotation, the weight #2 falls into the funnel through hole #B, etc... After weight #4 falls through hole #D of the square plate, four weights are again loaded.

When the weight dispenser is fully loaded, the total mass of the lead weights reaches 420 kg (4200 N). In order to avoid too much pressure on the rotating disk from the weights sitting on it, the helix is inclined at 10°, which limits the force on the disk to 730 N. Increasing the helix inclination helps the weights move downward in the pipes, but increases the pressure of the weights on the rotating disk. Conversely, if the slope is not strong enough, the weights can easily get stuck when the mooring line and the weight dispenser are tilted.

Accepted for publication in *Journal of Atmospheric and Oceanic Technology.* DOI 10.1175/JTECH-D-24-0009.1.

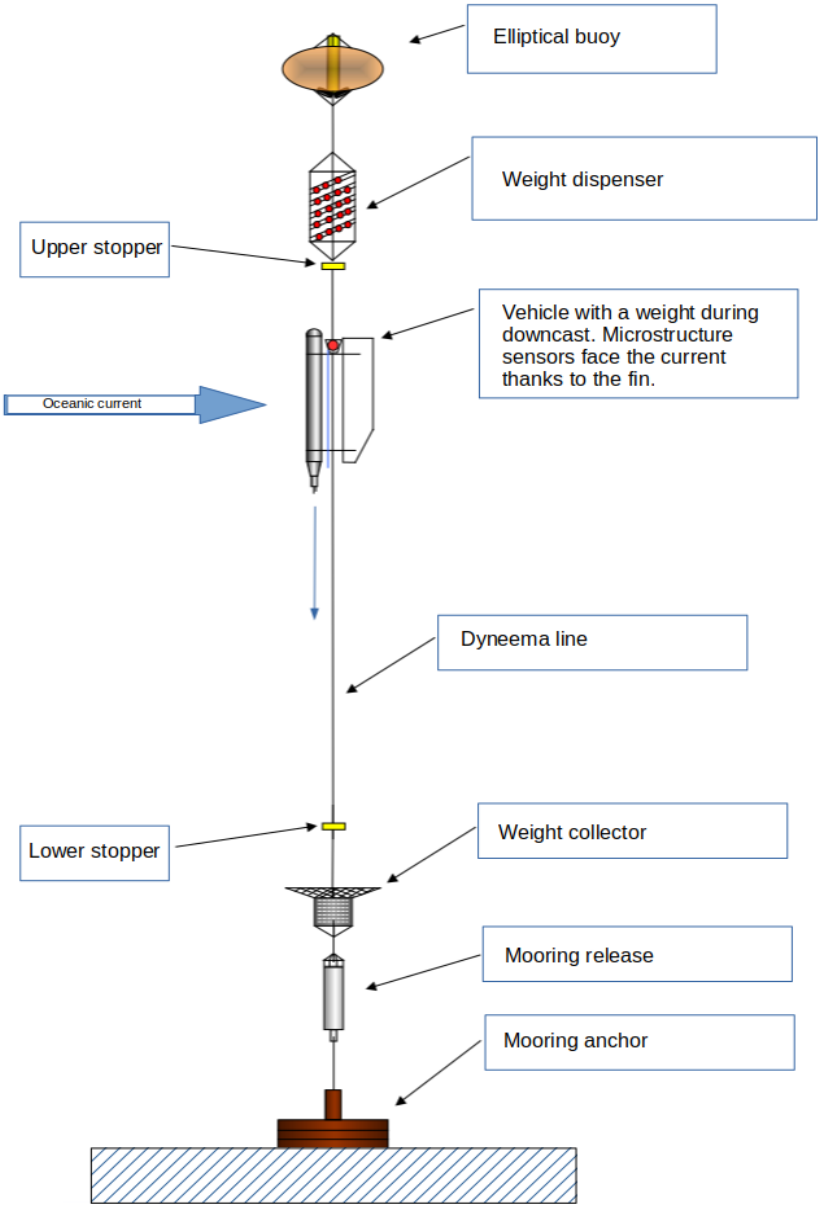

Figure 1 -MicroRiYo mooring schematic.

Accepted for publication in *Journal of Atmospheric and Oceanic Technology.* DOI 10.1175/JTECH-D-24-0009.1.

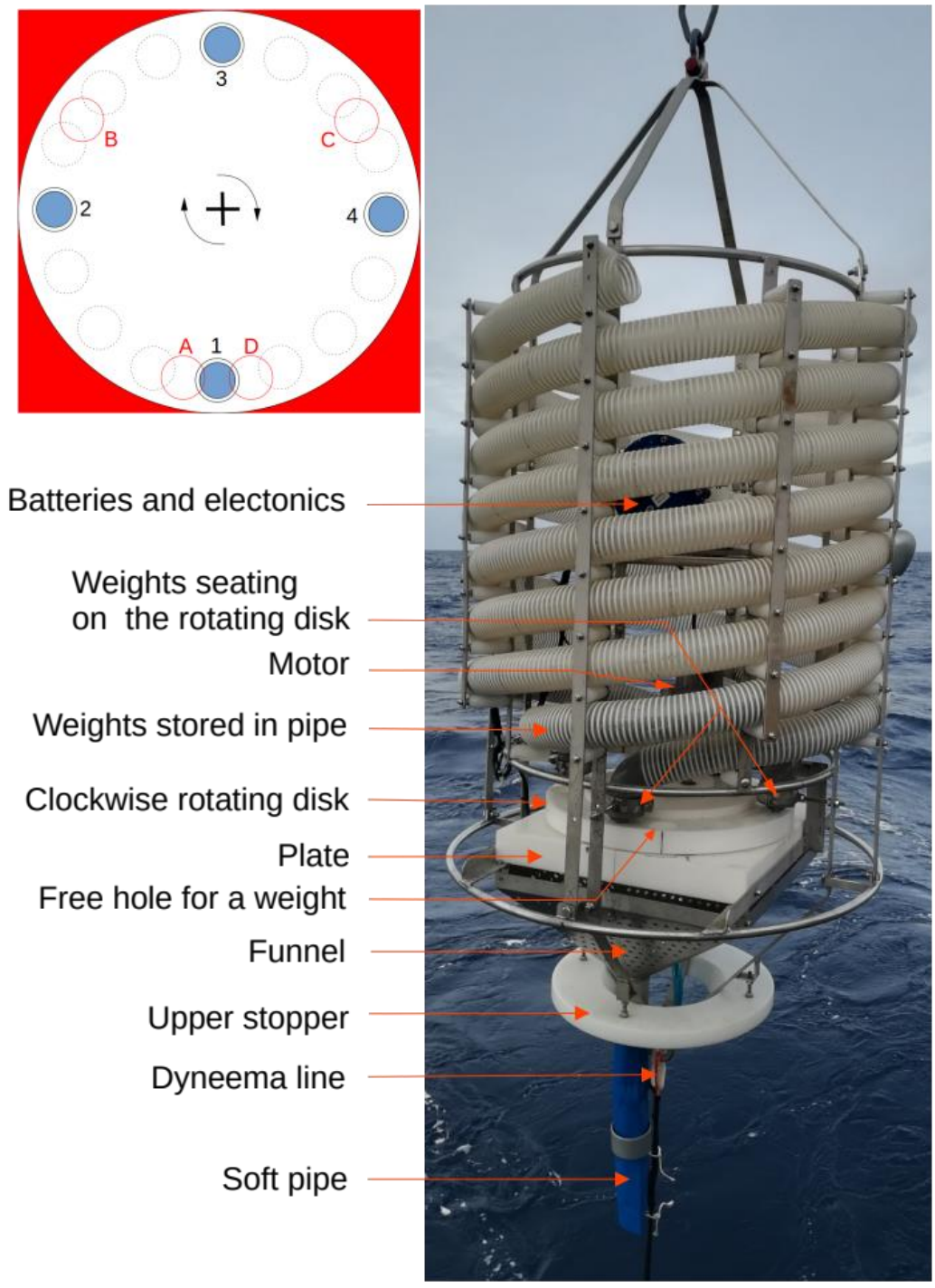

Figure 2 - Weight dispenser elements (right). Top view schematics of the rotating disk weight distribution (inset upper left): four weights (blue) are loaded in the evenly spaced holes 1-4 (solid black circles) of the rotating disk (white). The fixed unevenly spaced holes (A -D) of the square plate (red) successively receive a weight that falls in the funnel underneath at each 22.5° rotation. The positions of the holes 1-4 after each rotation are highlighted by the black dotted circles.

Accepted for publication in *Journal of Atmospheric and Oceanic Technology.* DOI 10.1175/JTECH-D-24-0009.1.

The rotating disk is triggered by a 12 V motor powered by a 10.8 V battery, consuming 0.46 mAh (5 mWh) per weight release. Inside the motor, is an internal triple cam arrangement that triggers four switches is used to precisely stop the rotation of the disk after a weight is released. The electronics count all switch state changes. After each full rotation of the disk, the counter is reset to zero to avoid any shift that caused by spurious oscillations of the switches. When the motor is not activated, the electronics enter a sleep mode that consumes only 0.018mAh (0.2 mW). The motor is powered by an 8 Ah (86 Wh) lithium battery, which provides enough power for more than 15 000 weight releases. When the release time is reached, the electronics test whether the vehicle is present under the weight dispenser. The presence sensor uses a reed relay located on the mooring line and a magnet on the vehicle basket. For this first deployment, the electronics were set to to release a weight every other release period if the vehicle was not detected. This was done in case of a failure of the presence sensor.

c. Vehicle

The vehicle moving along the mooring line is 302 cm long (Fig. 3). It consists of a water pipe (outer/inner diameter 16/14.1 cm) containing from top to bottom: syntactic foam buoyancy elements rated for 4000 m, a battery container rated for 4000 m, a MicroRider 6000 (MR, rated for 6000 m) wrapped with additional buoyancy elements. A fin is attached to the side of the pipe with two titanium bars to avoid contamination of the ocean turbulence with vortex shedding from the mooring line. Both the fin and the pipe are made of high-density polyethylene (HDPE), which has the advantage of having a slightly positive buoyancy in seawater (965 kg m^{-3}). The MR weighs 5.7 kg in seawater and the battery container 5.8 kg. With all the other small equipment, more than 14.1 kg of positive buoyancy must be added to obtain a positively buoyant vehicle. The total positive buoyancy added to the vehicle is 15.3 kg (including the HDPE elements). To balance the downcast and upcast velocities, an additional internal mass of 800 g is added to the vehicle, resulting in a total vehicle positive buoyancy of about 400 g for the upcast. For the downcast, the vehicle is negatively buoyant by about 900 g with the lead weight. These numbers are indicative; uncertainties exist and the weight of the cables is not taken into account.

The release of the weight is controlled by a fiberglass rod attached to the weight basket, and opposite end of which is below the lower titanium bar (Fig. 3). The lead weight, partially

Accepted for publication in *Journal of Atmospheric and Oceanic Technology.* DOI 10.1175/JTECH-D-24-0009.1.

enclosed by the weight basket, rests on the upper titanium bar in an unstable equilibrium. When the rod hits the stopper clamped to the mooring line, the weight basket moves upward and the lead weight simply falls off. This simple release system is designed so that a little more than 1 cm of rod lift is enough to release the weight.

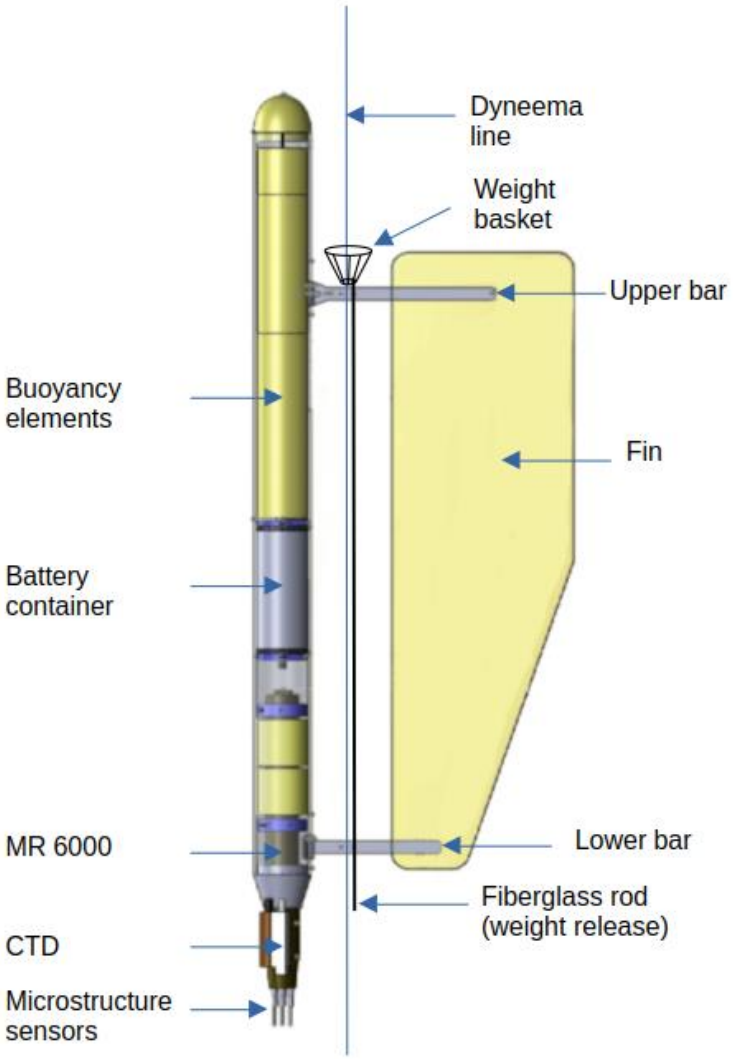

Figure 3 - MicroRiYo vehicle

d. MicroRider 6000 – Energy considerations

The MR is switched on when a lead weight falls into the basket located on the upper titanium bar. When the weight is in the basket, it pushes a tipping lever that closes a reed relay that turns the MR on. The MR is switched off and goes into a sleep mode (low power consumption) when either the weight in the basket falls off, or after a specified amount of

Accepted for publication in *Journal of Atmospheric and Oceanic Technology.* DOI 10.1175/JTECH-D-24-0009.1.

time. The latter condition prevents the MR battery from being drained if the MR gets stuck on the mooring line during its downcast. The time to powering down is 50% greater than the duration of a downcast at a nominal velocity.

When the MR is on and samples data, it consumes 2.5 W. A 2000 m profile at a mean downcast velocity of 0.5 m s^{-1} would require 2.8 Wh. If 300 profiles are to be done, a total of at least 830 Wh must be supplied. The battery container (5s 7p configuration of lithium D cells) contains roughly 1000 Wh, assuming that D cells have a conservative capacity of 8.5 Ah (temperature dependent).

e. Mooring line and anchor

The mooring line along which the vehicle moves is made of a racing Dyneema SK99, which has a breaking load of 6350 kg for a diameter of 7 mm. The Dyneema braid has a high strength, low UV sensitivity, low elongation, good creep, and is reusable. The positively buoyant elements on the mooring must compensate for the weight of the dispenser and provide sufficient tension to keep the mooring line as vertical as possible. The ground anchor is designed so that the mooring remains anchored to the ground if all the lead weights fall to the ground instead of falling into the collector. The mooring line passes through two Teflon rings screwed to each of the two titanium bars. To reduce the drag of the line passing through the rings during the vertical cast and the associated vibrations, the two rings are equipped with rollers that rotate when the line presses against them.

f. Deployment procedure

The vehicle remains a fragile assembly. In addition, it is equipped with fragile microstructure sensors that are easily broken if they hit the mooring line. The deployment of the mooring therefore starts with the anchor first, the ship holding its position. With the anchor first, the mooring line remains vertical and the various parts of the mooring are clamped onto the tensioned line. The line is paid out at a speed of 0.5 m/s until it reaches the location of the weight dispenser. At this location, there is no way to have a fixed grip on the

Accepted for publication in *Journal of Atmospheric and Oceanic Technology.* DOI 10.1175/JTECH-D-24-0009.1.

line over as the vehicle passes by for data sampling. Therefore, a 4-leg Yale Grip is used to stop the line and securely clamp the vehicle to the line. The vehicle is then deployed with a weight in its basket so that it begins to sink and does not stay at the surface in the waves and ship's wake. The Yale Grip is again used to clamp the dispenser. The mooring buoyancy is then attached. Finally, the mooring is deployed with a cable until the bottom of the mooring is 30-50 m above the seabed. The mooring is then dropped with an additional release attached to the cable. The most delicate phase of such a deployment is the clamping of the vehicle and the weight dispenser.

g. Specific configuration for this deployment

For this specific short-term deployment, the MR was constantly switched on, as the battery had enough power to last more than two weeks. To avoid the creation of a single large data file, the MR was set to start a new file every 2.5 h. The correct functioning of the tipping lever and associated reed relay, which in principle turns the MR on/off, was logged during the deployment. The weight dispenser was loaded with 70 lead weights and was programmed to release one weight every 5 hours.

At the top of this mooring, one elliptical and one spherical buoys provided an uplift force of +450 kg. It compensated for a total weight of -300 kg composed of the dispenser (-190 kg), the weight collector (-70 kg), the release (-20 kg) and the chains (-20 kg). The anchor weighed 400 kg.

The mooring was deployed to the north of the lava lake of the Lucky Strike segment of the Mid-Atlantic Ridge at a depth of 1715 m at 37.295°N and 32.279°W on June, 8th 2022 and recovered 15 days later. The lava lake is surrounded by three small seamounts that culminate around 1570 m. The vehicle profiled over 1075 m, between 620 m and 1695 m, stopping 20 m above the seafloor.

For comparison, fourteen Vertical Microstructure Profiler (VMP-6000) profiles were taken while the MicroRiYo was at sea. The VMP was deployed at an average distance of 120 m from the mooring. The mean estimated distance between the mooring and the end of the VMP downcast was 250 m. Most of the time, it was not possible to synchronize the VMP deployments with the MRY downcasts due to other operations at sea. On average, the VMP deployments took place two hours before or after the MRY downcasts, with a maximum time

Accepted for publication in *Journal of Atmospheric and Oceanic Technology.* DOI 10.1175/JTECH-D-24-0009.1.

difference of 5 hours. For safety reasons, the VMP was programmed to stop its downcast at 80 m above the seafloor, which was 60 m shallower than the end of the MRY downcast.

h. Performance

During this deployment, the vehicle collected 35 profiles out of the expected 70. This was due to a failure of the vehicle presence sensor after 23 hours, which forced a lead weight to be delivered every 10 hours instead of 5 hours.

The mean and standard deviation of the vehicle downcast velocity is 0.63 ± 0.04 m s^{-1}. A few profiles or sections of profiles show slower downcast velocities around 0.5 m s^{-1} (Fig. 4). No relationship was found between the vehicle downcast velocity and the horizontal current magnitude ranging from few to 25 cm s^{-1}, as measured by a 38 kHz Ship Acoustic Doppler Current Profiler (SADCP) sampling down to 1400 m (not shown).

Three MRY profiles were selected to verify that the vehicle fin was oriented in the direction of the current. These three vehicle profiles occurred within less than 15 minutes of Lowered Acoustic Doppler Current Profiler (LADCP) profiles taken 400 m south of the mooring position. SADCP profiles are also used to check the consistency of the measurements. While the fin is oriented in time an space with the local meter-scale currents, the LADCP and SADCP profiles are constructed from averages of raw data in the vertical, horizontal and in time. Overall, the orientation of the fin is consistent with the direction of the current (Fig. 5). Sometimes, the agreement is better with the LADCP profile and sometimes with the SADCP profile. As a result, the shear sensors are not impacted by the vortex shedding created by the horizontal current interacting with the mooring line, as these vortices are generated downstream of the shear sensors.

Accepted for publication in *Journal of Atmospheric and Oceanic Technology.* DOI 10.1175/JTECH-D-24-0009.1.

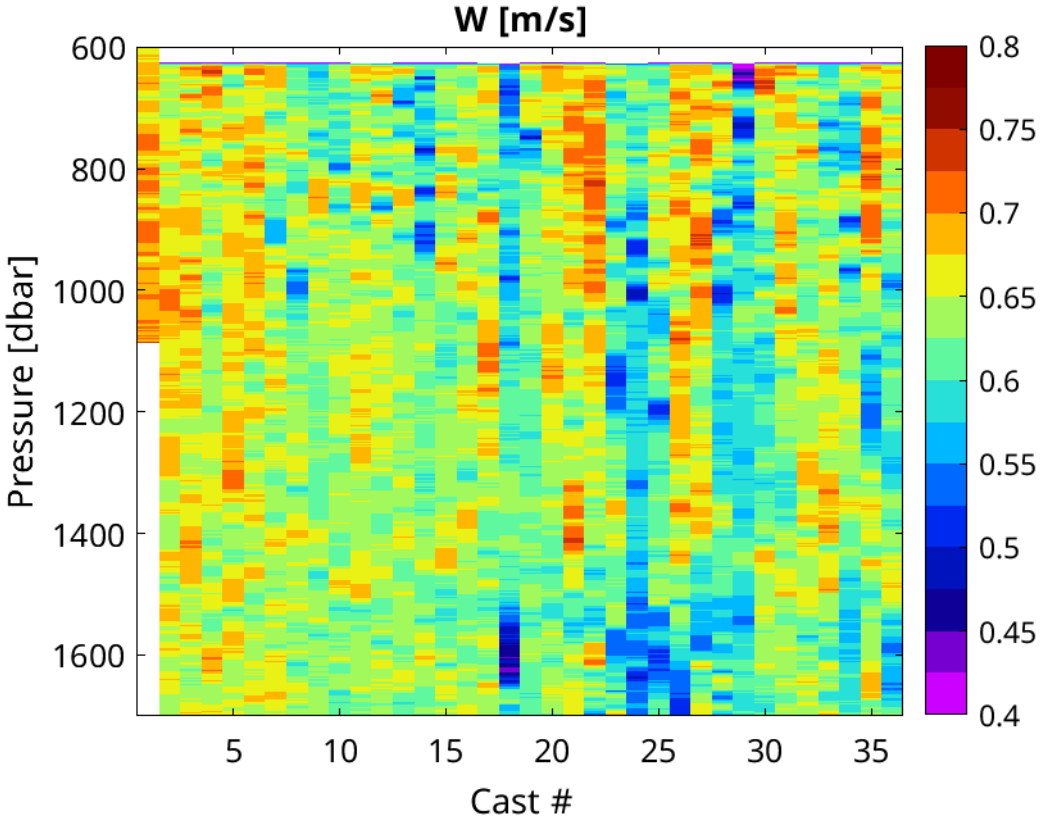

Figure 4 - Vertical velocity of the vehicle during downcasts. Note that the first cast occurred during the mooring deployment and thus stopped at a shallower depth of 1090 dbar. Excluding this first cast, the mean and standard deviation velocity is 0.63± 0.04 m/s. Few profile segments exhibit a slower velocity around 0.5 m/s.

3. Data quality

The shear data from the MicroRiYo followed the same processing as the VMP shear data to get dissipation rates: first, spikes were removed from the raw shear data, then vibrations contaminating shear data were removed using spectral coherence between velocity shear data and accelerometer data over 8 s segments (Goodman et al. 2006; Ferron et al. 2023). The shear variance was estimated by averaging 2 s FFTs half-overlapping over the 8 s segments. Note that 2 s of data represents a vertical distance of about 1.30 m, nearly half the vehicle length, and provides a wavenumber low enough to resolve the dissipation spectral range in weakly turbulent environments. For more details on shear data processing, the reader is referred to the processing flowchart of the Atomix SCOR Working Group 160 that we have

Accepted for publication in *Journal of Atmospheric and Oceanic Technology.* DOI 10.1175/JTECH-D-24-0009.1.

followed for dissipation rate estimation (https://atomix.app.uib.no/Flow_chart_for_shear_probes). Note that the Atomix group has some recommendations for the quality control of the dissipation rate estimates that use statistics of the despiking process, agreement between dissipation rates from redundant sensors, and a figure of merit (our criterion 10 below)(https://atomix.app.uib.no/Shear_probes_quality_control_metrics). Here, our shear data are almost free of spikes (the advantage of deep-sea measurements) and the two shear sensors are consistent. We have strengthened the shear quality control by adding other criteria, mostly aimed at detecting spectral weaknesses in weakly turbulent environments.

Accepted for publication in *Journal of Atmospheric and Oceanic Technology.* DOI 10.1175/JTECH-D-24-0009.1.

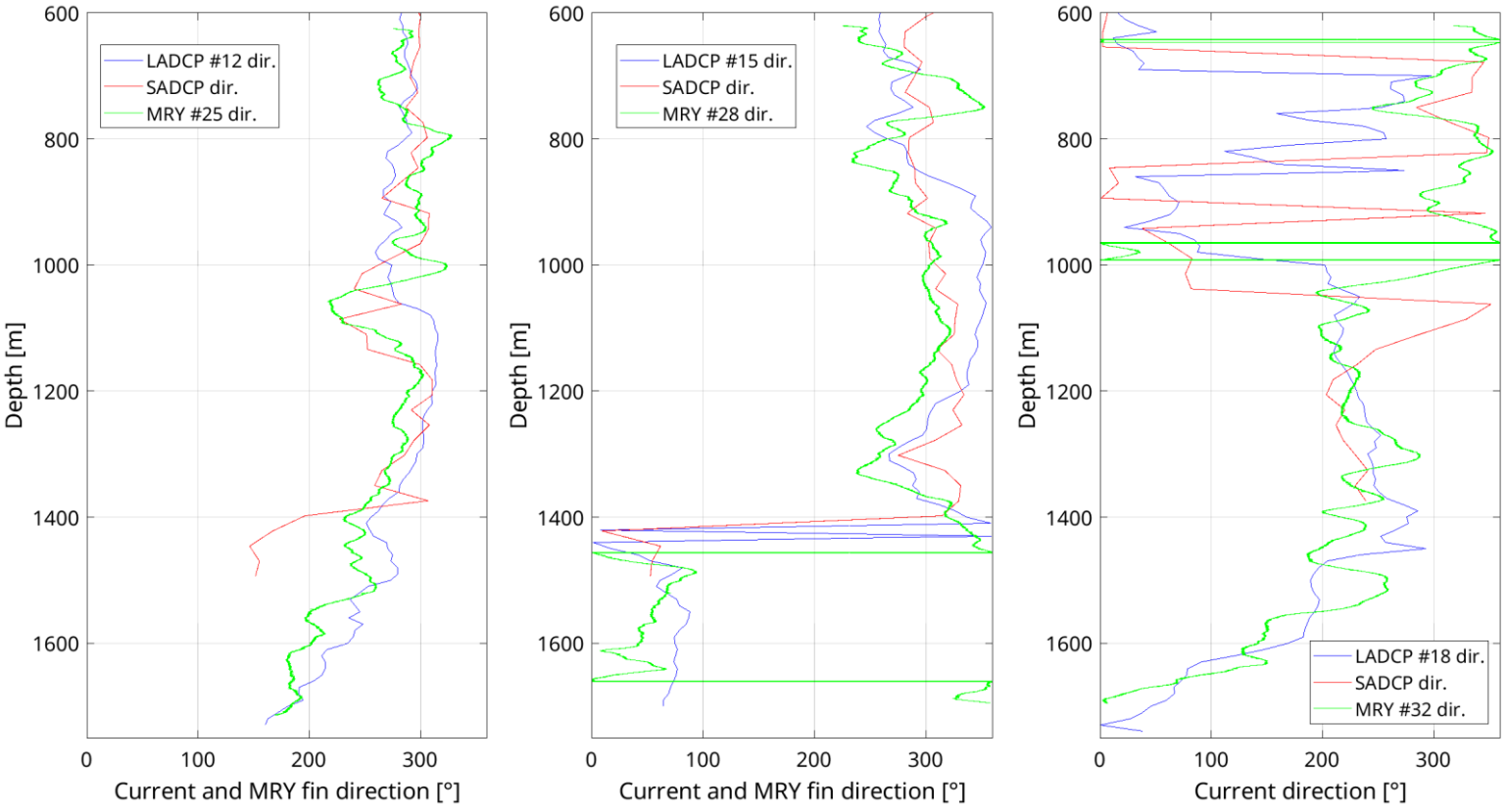

Figure 5: Comparison of the direction of the vehicle fin (MRY) with the direction of horizontal current as estimated by the Lowered-ADCP (LADCP) and the Ship-ADCP (SADCP) . For those three casts, the LADCP profile and the MicroRiYo vehicle profile occurred within less than 15 minutes. The fin is expected to orient along the current direction.

Accepted for publication in *Journal of Atmospheric and Oceanic Technology.* DOI 10.1175/JTECH-D-24-0009.1.

The quality of the shear data was examined by assessing the quality of the fit of the observed shear spectra, P_{shear}, to the theoretical Nasmyth spectrum, $P_{Nasmyth}$. In practice, the ratio of the two spectra, $R_P = P_{shear} / P_{Nasmyth}$, were examined over the spectral range used for the variance calculation using the following 10 criteria:

1. R_P should not be biased by more than a factor f_m, i.e. $|< \log_{10} R_P >| < \log_{10} f_m$, with $f_m = 1.25$, $<>$ denotes an average over the spectral range.
2. The typical departure from the perfect fit ($R_P = 1$) should remain smaller than a factor f_d, i.e. $\text{median}(|\log_{10} R_P|) < \log_{10} f_d$, with $f_d = 2$ and the median calculated over the spectral range. The mean of three largest spectral departures from the Nasmysth spectrum over the first half of spectral range should stay smaller than 4: $|\max_3(\log10(R_p))| < 4$.
3. At low wavenumbers, R_P should not be biased by more than a factor f_h, i.e. $|< \log_{10} R_P >_{low}| < \log_{10} f_h$, with $f_h = 1.5$ and $<>_{low}$ denotes an average over the first half of the spectral range.
4. At high wavenumbers, R_P should not be biased by more than a factor f_h, i.e. $|< \log_{10} R_P >_{high}| < \log_{10} f_h$, with $f_h = 1.5$ and $<>_{high}$ denotes an average over the second half of the spectral range.
5. The percentage of the spectral components over the first half of the spectral range that depart from the Nasmysth spectrum by a factor larger than 3 should remain smaller than 20%.
6. Departures over several consecutive spectral components should remain sufficiently small: filter $\log10(R_p)$ using a moving median over 4 spectral components (mov_median_4) to remove local spectral departures and check whether: $<|\text{mov\_median}_4(\log_{10}(R_P))|> < \log_{10}(1.6)$.
7. The drop of the shear spectra between the low and the high wavenumber part of the spectral range should not depart by more than a factor of 3 from the spectral drop of the Nasmyth spectrum.
8. At least 70% of the shear spectra should be resolved from the lowest wavenumber to the Kolmogorov wavenumber.

Accepted for publication in *Journal of Atmospheric and Oceanic Technology.* DOI 10.1175/JTECH-D-24-0009.1.

9. For each spectra, the standard deviation of the difference between the shear and the Nasmyth spectrum should remain smaller than the expected standard deviation times a factor of 1.1 (Lueck 2022, Eqns 22 and 24; see also https://atomix.app.uib.no/Figure_of_merit).

The values set for each criterion are arbitrary and were determined after several attempts for low dissipation rates (typically, $\varepsilon < 10^{-8}$ W/kg) encountered in the open ocean, which span low wavenumbers. Each criterion is designed to test a specific characteristics of the shear spectrum; the criteria are not independent of each other, but none are equivalent. If 80% of the 10 criteria are met for a shear spectrum, the spectrum was considered as good with respect to the Nasmyth spectrum. If this percentage is less than or equal to 60%, the spectrum is suspect. A suspect spectrum requires further investigation and can be discarded by comparing it to neighboring good spectra (either from the same or a different shear sensor). The percentages of passing criteria are helpful in diagnosing problems that are not always easy to detect by looking at the dissipation rates alone and without having to check thousands of spectra. In this study, all spectra that did not meet 80% of the criteria were discarded. No rejection was based solely on failure to meet a given criterion. The value checked for a given criterion and the result (criterion passed or failed) are recorded in the output file for each dissipation rate estimate. This makes it easy for a user to add other rejection criteria later.

In the following, we selected the 14 MRY profiles that were closer in time to the 14 VMP profiles (see section 2g). The 14 MRY profiles are used to examine the statistics of the criteria, which are compared to the VMP. For these 14 profiles (typically 900 spectra per profile), the median percentage of good spectra for a VMP profile is 87% (Fig. 6 left panel, dashed lines). The median percentage of good spectra for a MRY profile is the same (88%; Fig. 6 left panel, solid lines). The two shear sensors of the MicroRiYo profile #4 provided poor data quality for reasons that are unclear. Although the MicroRiYo was not serviced during its deployment at sea, the data quality returned to normal after profile #4. However, the last profile from the MicroRiYo showed worse spectra for shear #2 (53%) and to a lesser extent for shear #1 (76%).

Accepted for publication in *Journal of Atmospheric and Oceanic Technology.* DOI 10.1175/JTECH-D-24-0009.1.

Among all the spectra of the 14 profiles, the percentage of success for each criterion is greater than 80%, except for criterion #9, which is based on the resolved percentage of the spectral range, which is more restrictive (50-55% of success, Fig. 6 right panel). For the VMP profiles, the criterion #5 is lower than for the MicroRiYo because of the first 4 VMP profiles that used old shear sensors.

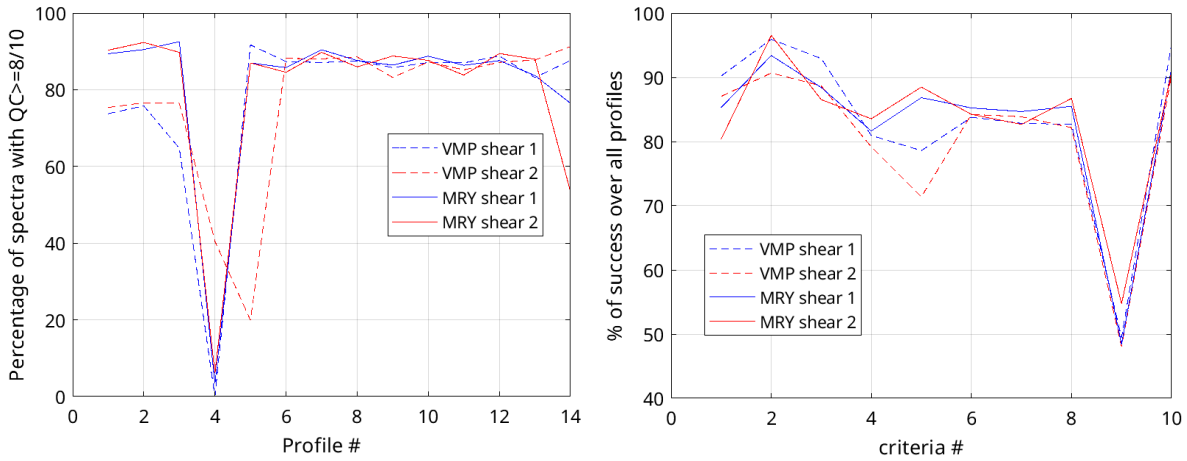

Figure 6 : (left) Percentage of "good" spectra that successfully passed at least 8 of the 10 shear spectra quality check criteria (see text) as a function of the profile #; each profile counts ~900 spectra. (right) Percentage of success for each quality check criteria calculated over all the profiles (~12600 spectra).

The 14 VMP profiles were deployed at a distance of 90 to 190 m to the south of the MRY mooring (see D_{dep}, title of Fig. 7, second row). Four VMPs (#7, 10, 12, 13) reached 630 dbar synchronously with the start of the MRY profile at the same pressure (pressure at the location of the weight dispenser)(see T_{dep}, title of Fig. 7, first line). Once deployed, the VMP drifted with the currents without being tracked. However, the GPS position at which the VMP surfaced allowed its position at the deepest part of its downcast to be estimated. The distance between the closest VMP position to the bottom and the MRY mooring line was estimated to be between 140 and 380 m (see D_{bot}, Fig. 7). Note that the estimated VMP position near the bottom from the GPS data is consistent with a simple drift model using LADCP currents measured at the nearby CTD stations.

Whether the dissipation rate is measured with the VMP or the MRY, it shows a large variability from profile to profile, often reaching one order of magnitude between 600 – 1400

Accepted for publication in *Journal of Atmospheric and Oceanic Technology.* DOI 10.1175/JTECH-D-24-0009.1.

dbar, and two orders of magnitude below 1400 dbar (Fig. 7). Interestingly, the most synchronous profiles (VMP #7, 10, 12, 13; MRY #25, 28, 30, 32) are also those that show the best consistency in the vertical variability of ε between the VMP and the MRY.

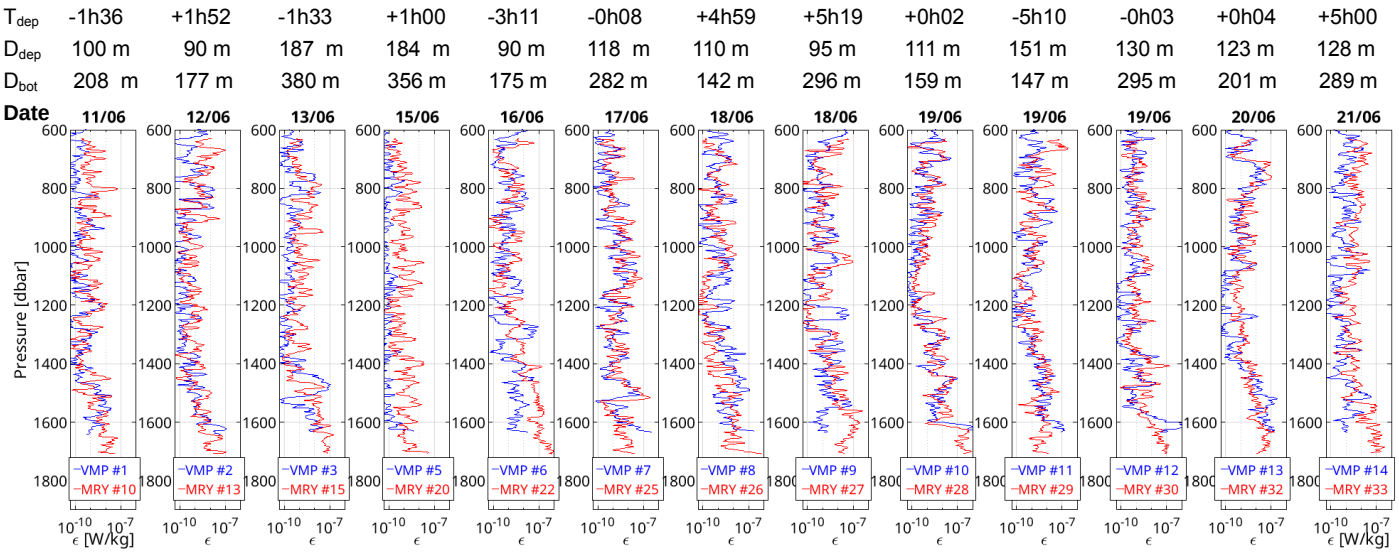

Figure 7: Comparison of 13 dissipation rate profiles as measured by the MicroRiYo vehicle (red, MRY) and the VMP (blue)(units W kg $^{-1}$). Title of the figure: time between VMP deployment and the start of MRY profile at 630 dbar (T_{dep}, upper line, -/+ = VMP deployed before/after MRY), distance between VMP deployment and MRY mooring line (D_{dep}, middle line, deployments were to the south of the MRY mooring), distance between mooring line and VMP at the end of its downcast (D_{bot}, lower line), profile date.

Therefore, we use these four synchronous profiles to assess the quality of the dissipation rate estimates. For each profile, the FFT segments were binned by dissipation rate ranges, going from $1 – 5 \times 10^{-10}$ W kg^{-1} to $1 – 5 \times 10^{-7}$ W kg^{-1}. For a given MRY profile, the median of the acceleration spectra, the magnitude-squared coherence between shear and acceleration, and the shear spectra of the FFT segments falling within a dissipation range are shown in Fig. 2 for MRY profiles #28 and 32, which span the largest dissipation rate ranges.

For profile #28, the vibration-cleaned shear spectra (solid lines) fit the Nasmyth spectra (dashed lines) as they exhibit a significant drop after 10 Hz, even for ε as low as 2.6×10^{-10} W kg^{-1} (Fig. 8, upper left panel). Horizontal accelerations in the fin plane (a_x) and orthogonal to the fin plane (a_y) show increased variance above 10 Hz (a_x) and 20 Hz (a_y). Below these frequencies, the variance exhibits a few peaks at 1, 4 and 8 Hz for a_x, and at 3, 7 and 11 – 13

File generated with AMS Word template 2.0

Accepted for publication in *Journal of Atmospheric and Oceanic Technology.* DOI 10.1175/JTECH-D-24-0009.1.

Hz for a_y. Irrespective of ε, the magnitude-squared coherence (hereafter coherence) between shear and acceleration is weak for a_x below 10 Hz. For a_y, the coherence peaks above 0.8 for ε below 5×10^{-9} W kg^{-1}. The weaker the ε, the larger the coherence at 3, 7 and 11 Hz as the amplitude of the ocean shear signal decreases. Thus, vibrations must be removed from the raw shear spectra at these low dissipation rates to avoid overestimating ε. The amplitude of the vibration removal is conveyed by the variance decrease between the raw (colored dots) and the clean spectra. After cleaning, the MRY spectra converge within a factor of two to the VMP spectra (black lines) calculated over the same segment depths for the two smallest dissipation ranges (magenta and blue lines). For larger MRY dissipation ranges, which count fewer segments than for weak ε, the median of ε estimated from the VMP at the same depth segments remains within a factor of 3 to 4.

As a second example, the cleaned shear spectra of profile #32 show a worse fit to the Nasmyth spectrum as the spectral drop is weak for the two smallest dissipation ranges (Fig. 8, lower panels). The variance of the acceleration is not worse than for profile #28 and the coherence is even weaker than for profile #28. A criterion could be added to filter out or flag cleaned shear spectra that do not resolve the spectral roll-off sufficiently well (i.e filter spectra that are too flat at low dissipation rates). For larger dissipation ranges, the shear spectra fit the Nasmyth spectra as in profile #28. Despite the lower quality of the MRY spectra, the medians of ε from the VMP over the three weaker dissipation ranges remain within a factor of 2 of those from the MRY. For the largest dissipation range measured on this MRY profile (median ε of 1.1×10^{-7} W kg^{-1} for the range $1 - 5 \times 10^{-7}$ W kg^{-1}), the median ε from the VMP on the same segment depths is fifteen-fold less. This dissipation range is populated by only 6 segments and the statistic is not reliable as the VMP and the MRY, 200 m apart, may encounter different patches of enhanced turbulence.

We now examine how the downcast velocity relates to the acceleration and shear at low dissipation ranges where the signal-to-noise ratio is low. Attention is focused on the spectral characteristics below 10 Hz, which represents a large portion of the spectral integration range for small dissipation ranges. For MRY profile #25 and for the dissipation range $1 - 5 \times 10^{-10}$ W kg^{-1}, the variance of the horizontal acceleration in the direction of the fin (a_x) tends to increase at low frequencies (1, 4, 8 Hz) with lower downcast velocities (Fig. 9, upper left

Accepted for publication in *Journal of Atmospheric and Oceanic Technology.* DOI 10.1175/JTECH-D-24-0009.1.

panel, dashed lines). However, this increase is not systematic. For instance, the variance below 3 Hz is the weakest for the smallest downcast velocity but peaks at 4 – 5 Hz. In the horizontal orthogonal direction, the variance in a_y below 10 Hz peaks sometimes for the smallest velocities and sometimes for the largest velocities (Fig. 9, upper left panel, solid lines). For the following dissipation range ($1 – 5 \times 10^{-9}$ W kg^{-1}), the three smallest velocities exhibit a peak at 1 Hz in a_x, the smallest velocity has the highest variance at 4 Hz, and the largest downcast velocity still has the lowest variance below 10 Hz (Fig. 9, upper right panel). Note that the peak at 8 Hz, clearly visible in a_x for the two dissipation ranges at velocities of 0.5 m s^{-1}, increases in frequency to 10 – 11 Hz as the downcast velocity increases to 0.7 m s^{-1}, which is expected for vortex shedding from a small structure facing a flow. For MRY profile #32, which contrasts with MRY #25, the variance in a_x and a_y below 10 Hz decreases by a factor of two to three for the largest downcast velocity and for all frequencies below 10 Hz (Fig. 10). For a_y, there is no specific ordering of the spectral variance peaks as a function of the downcast velocity similarly to MRY #25.

For MRY #25 and for the lowest dissipation range ($1 – 5 \times 10^{-10}$ W kg^{-1}), the coherence between shear and a_x is always below 0.4 below 10 Hz, regardless of the downcast velocity, except for a peak at 4.5 Hz at a velocity of 0.55 m s^{-1} (Fig. 9, middle left panel). Contrastingly, the coherence between shear and a_y is large at small downcast velocities, reaching values above 0.9 at 0.55 m s^{-1}. This coherence tends to decrease with increasing downcast velocity: peaks above 0.8 are still present, but cover a smaller frequency range below 10 Hz. For the following dissipation range ($1 – 5 \times 10^{-9}$ W kg^{-1}) and below 10 Hz, the coherence between shear and a_y decreases in both amplitude and frequency range as the ocean turbulence signal increases and masks the influence of spurious vibrations (Fig. 9, middle right panel). Below 6 Hz, peaks of coherence above 0.8 concern only the smallest downcast velocity (0.5 m s^{-1}). Coherence peaks above 0.8 around 8 Hz and 11 Hz are present regardless of velocity.

The presence of a large coherence at small downcast velocities is indicative of the influence of vibrations on shear measurements in weakly turbulent environments. Vibrations originate from vortex shedding and friction of the vehicle on the mooring line. These vibrations vary from profile to profile as MRY #32 contrasts with MRY #25 with a weaker coherence magnitude (Figs. 9 and 10). Removing the vibrations from raw shear spectra is a prerequisite before estimating a dissipation rate.

Accepted for publication in *Journal of Atmospheric and Oceanic Technology.* DOI 10.1175/JTECH-D-24-0009.1.

To quantify whether the vibration removal is efficient even in cases where coherence is large at small downcast velocities and small ε, we compare the cleaned MRY spectra to the VMP spectra obtained at the same depth segments. For MRY#25 and a dissipation range of $1 – 5 \times 10^{-10}$ W kg^{-1}, the cleaned spectra exhibit a good spectral drop, especially at low downcast velocities (Fig. 9, lower left panel). However, compared to the Nasmyth spectra, they have too much variance below 1.5 Hz, but this does not bring much excess variance when integrating over the whole spectral range to obtain the dissipation rate. The VMP spectrum (black line) is close to those of the MRY as the VMP median dissipation rate is equal to that of the MRY (3.0×10^{-10} W kg^{-1}). All spectra collapse to the same variance between 2 and 6 Hz. For the following dissipation range ($1 – 5 \times 10^{-9}$ W kg^{-1}), the MRY-cleaned shear spectra are consistent regardless of the downcast velocity (Fig. 9, bottom right panel). The agreement with the VMP spectrum is good and the dissipation rate from the two platforms is within a factor of two. For the MRY #32 profile, which has a lower shear-acceleration coherence, the MRY-cleaned spectra have a less good fit to the Nasmyth theoretical form, as the spectral drop is not marked for the smallest dissipation range (Fig. 10, lower left panel). For the following dissipation range, the MRY-cleaned shear spectra fit the Nasmyth spectra better but the fit is not as good as for MRY #25 (Fig. 10, lower right panel). The VMP spectrum is consistent with the MRY spectra and the dissipation rate remains within a factor of two between the two instruments. With these observations in mind, the noise level of profiles #25 is in the range of $1 – 5 \times 10^{-10}$ W kg^{-1}, while that of profile #32 is in the range of $1 – 5 \times 10^{-9}$ W kg^{-1}.

4. Advantages, limitations and possible improvements

a. Advantages

This mooring minimizes the amount of energy required from batteries. In fact, no batteries are needed to move the vehicle, except for the 0.46 mAh used by the 12V motor of the weight dispenser to drop a weight on the vehicle and start a profile. The motion of the vehicle itself is then induced only by its negative and positive buoyancy. A clear advantage is that a 2000 m long profile has the same energy cost (i.e. one weight release) for vehicle motion (but not for data collection) as a 200 m long profile. In addition, the weights used to move the vehicle are recovered with the mooring at the end of the deployment. These features make the vehicle environmentally friendly.

Accepted for publication in *Journal of Atmospheric and Oceanic Technology.* DOI 10.1175/JTECH-D-24-0009.1.

Since there is no motor to move the vehicle, a potential source of vibration that could potentially contaminate the shear spectra is removed. The use of quasi-freefall downcasts is the best way to get the cleanest shear data possible, just like the VMP-6000.

Compared to the VMP-6000, which stops its downcast 60 – 90 m above the seafloor, the MRY allows measurements of dissipation rates closer to the seafloor. An optimized mooring configuration should allow the MRY to measure dissipation rates as close as 10 – 15 m from the seafloor. This is a clear advantage for better assessing the temporal variability of dissipation rates, mixing efficiency and buoyancy fluxes near the seafloor.

b. Limitations

Due to its design and size, the mooring is more appropriate for deep environments. For shallower depths, other lighter systems such as the Wirewalker may be more appropriate. Note that for depths shallower than 1000 m, the use of a buoyancy neutral Microrider-1000 would reduce the size of the vehicle and/or increase the payload of the vehicle for additional sensors.

Above a yet to be determined threshold of horizontal current magnitude, the vehicle will get stuck on the mooring line due to the increased friction between the mooring line and the vehicle. This may also happen if the tilt of the mooring line is too large. The slower the profiling speed, the easier it is for the vehicle to get stuck. During this deployment, the horizontal currents were low enough (<= 0.25 m s^{-1}) to avoid such sticking during the downcast. However, the vehicle upcast speed (0.15 m s^{-1}) was too slow and the vehicle remained stuck for tens of minutes to five hours on some profiles.

Accepted for publication in *Journal of Atmospheric and Oceanic Technology.* DOI 10.1175/JTECH-D-24-0009.1.

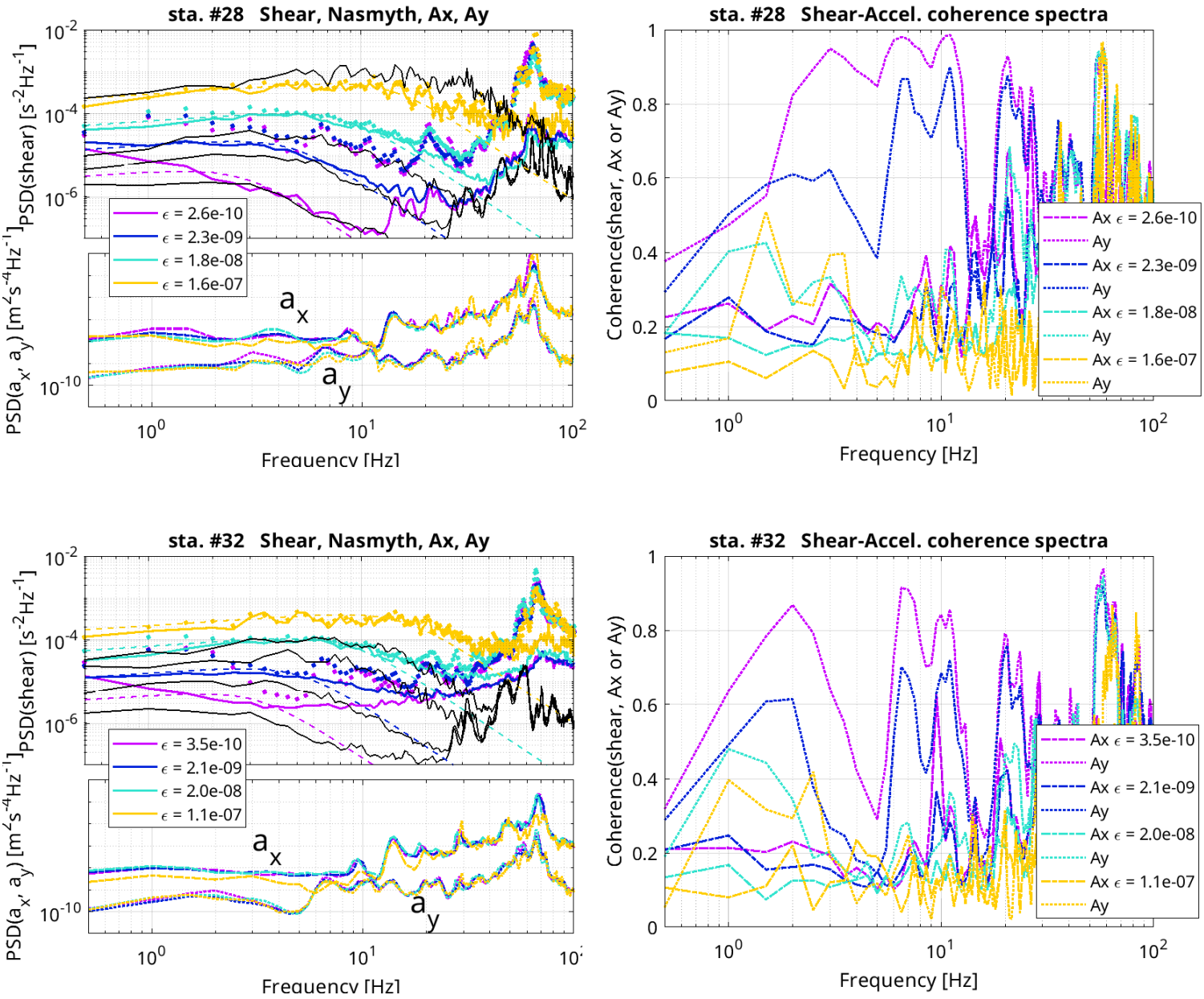

Figure 8: (upper row, left) MRY median shear and uncalibrated acceleration (a_x dashed, a_y dotted) spectra of dissipation rates falling in the ranges $1 – 5 \times 10^{-10}$ W kg^{-1} to $1 – 5 \times 10^{-7}$ W kg^{-1}, and (right) associated magnitude-squared coherence between shear and acceleration for MRY #28. On the shear spectra, dots show the raw spectra, solid lines are the spectra cleaned from vibrations, dashed lines are the Nasmyth fit to the cleaned spectra, and black lines denote the median VMP spectra among the MRY depths identified for a specified dissipation range. Dissipation rates in the legend are medians within the bin range.

Accepted for publication in *Journal of Atmospheric and Oceanic Technology.* DOI 10.1175/JTECH-D-24-0009.1.

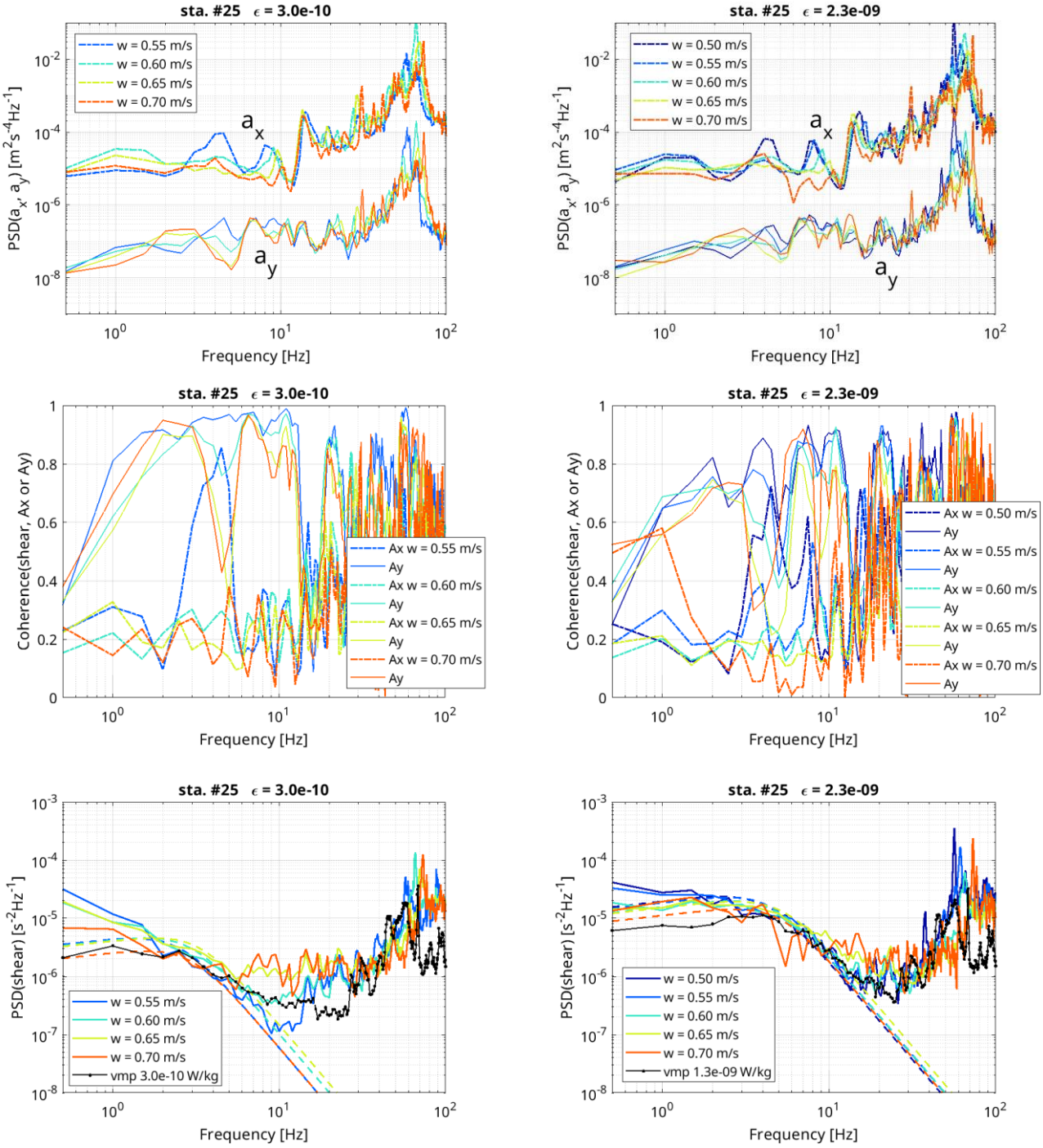

Figure 9: Some spectral characteristics of MRY profile #25. (upper row) MRY median spectra of uncalibrated acceleration in the horizontal plane (a_x, dashed line, is in the direction of the fin; a_y, solid line, is orthogonal to the fin plane), (middle row) MRY median shear-accelerometer magnitude-squared spectral coherence, (lower row) MRY median cleaned shear spectra. The median is calculated among all occurrences belonging to 1) a vehicle downcast velocity range (range of 0.05 m/s centered on the velocity appearing in the figure legend and highlighted by a line color), and 2) a dissipation rate in the range $1 – 5 \times 10^{-10}$ W kg^{-1} (left column) or $1 – 5 \times 10^{-9}$ W kg^{-1} (right column). The shear spectra from VMP (lower row, black line) is the median of the nearby VMP profile for the same depth segments as those selected for the MRY.

File generated with AMS Word template 2.0

Accepted for publication in *Journal of Atmospheric and Oceanic Technology.* DOI 10.1175/JTECH-D-24-0009.1.

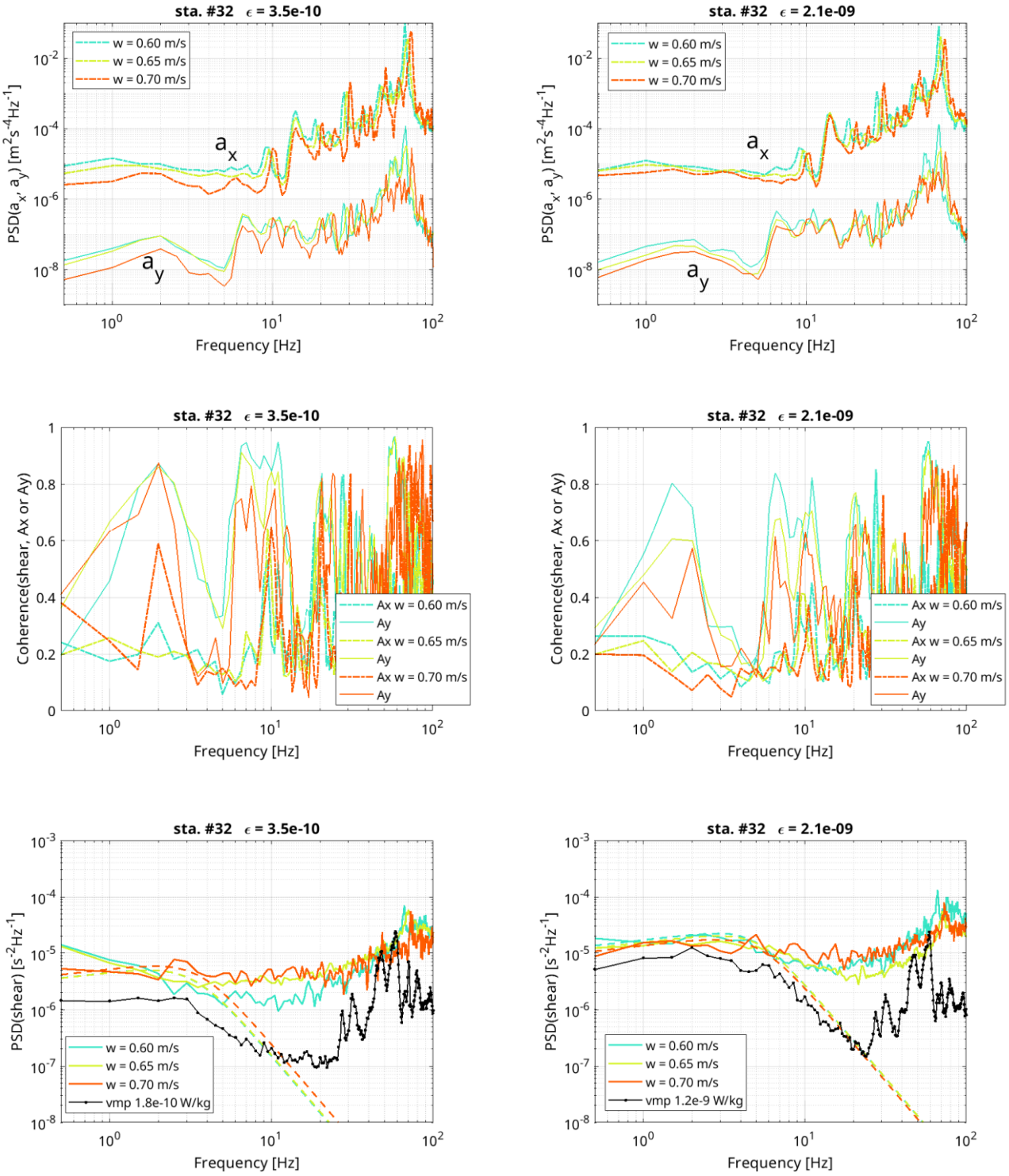

Figure 10: Same as Fig. 9 for MRY profile #32.

Accepted for publication in *Journal of Atmospheric and Oceanic Technology.* DOI 10.1175/JTECH-D-24-0009.1.

The time between two profiles cannot be less than the time required for the vehicle to return. Thus the frequency of the microstructure profiles is constrained by the downcast (lead weight) and upcast (floating buoyancy elements) velocities and by the length of the mooring line. Depending on the dynamics that is to be captured, the user must play with these three parameters to achieve the desired sampling frequency.

c. Possible adjustments and improvements

To reduce the number of vehicle stops during the upcast, the upcast velocity must be increased by slightly decreasing the additional internal mass of 800 g added to the vehicle. Conversely, the downcast velocity will decrease. Achieving an upcast velocity of 0.3 m s^{-1} and a downcast velocity of 0.5 m s^{-1} has proven successful in previous tests (cruises MICROCO and LOPSTECH in the Mediterranean Sea). A slower downcast velocity reduces the vibrations associated with the vehicle motion, which is beneficial for shear data quality. Such velocities were not achieved during this cruise because some parts were replaced and others added compared to previous cruises (e.g. stainless parts replaced by titanium).

Dissipation rate profiles obtained with this mooring show a noise level that varies between O(10^{-10}) W kg^{-1} and O(10^{-9}) W kg^{-1}. This noise level is low enough to highlight turbulent patches at depth, but it could be lowered by decreasing the spectral coherence between vibrations and shear at low frequencies. Improving the signal-to-noise ratio in weakly turbulent environments remains a challenge because of the need to attenuate low-frequency vibrations. One possibility, not yet explored, is to add silent blocks at the junction of the titanium bars and the HDPE pipe that would absorb some of the low-frequency vibrations (1 – 10 Hz). Another possibility is to add a system of four rollers to the ring of the titanium bars where the mooring line passes through. The system currently use two rollers, which has proven helpful in slightly increasing the downcast and upcast velocities by reducing the friction between the mooring line and the vehicle.

Accepted for publication in *Journal of Atmospheric and Oceanic Technology.* DOI 10.1175/JTECH-D-24-0009.1.

During this deployment, the presence sensor failed after 23 hours due to excessive stress on the reed relay. Indeed, the ocean currents move the vehicle in such a way that even a small displacement of the vehicle by 1 – 2 cm (either vertically or horizontally) will change the distance between the reed relay and the magnet and possibly activate or deactivate the switch. The record showed that the reed relay changed its state at a high frequency (a few seconds or less) for long periods of time, which finally broke its mechanical system after several thousand state changes. The difficulty is that the reed relay must be activated by the magnet at a very short distance. Increasing the strength of the magnet would increase this distance but it would also increase the risk of breaking the relay's mechanics due to the stronger magnetic field. To overcome these limitations, the reed relay must be replaced with another technology. We are currently testing the Radio Frequency Identification (RFID) technology, which has a larger distance of activation than the reed relay. This involves replacing the magnet on the vehicle with a "low" frequency 125 kHz RFID tag (transponder). The reed relay is replaced by an RFID antenna that located under the weight dispenser. In seawater and at a frequency of 125 kHz, the penetration depth, i.e. the reading distance at which the tag is detected by the antenna, reaches several tens of centimeters depending on the size of the antenna, its electronics and the size of the tag. Such a distance is a clear advantage over the magnet and reed relay. Another obvious advantage of RFID technology is that there are no mechanical parts to break as there are with the reed relay. A disadvantage is that the antenna requires a power supply. To avoid keeping the antenna permanently powered and ro save energy, the antenna is only activated from time to time and for about 10 seconds to check if the tag on the vehicle is nearby before releasing a weight. The MicroRiYo mooring was deployed with the RFID solution for one year during the CROSSROAD cruise, which took place in August 2024.

Acknowledgments. The development of the MicroRiYo benefited from several test cruises in the Mediterranean sea and the Atlantic Ocean: ESSLOPS 2017 (DOIs: 10.17600/17005100, 10.17600/17005500), Microco 2018 (DOI: 10.17600/18000601), LOPSTECH 2019 (DOI : 10.17600/18000917), MoMARSat 2020, 2021, 2022 (DOIs: 10.17600/18000684, 10.17600/18001296, 10.17600/18001914). We thank the crew members from the N/O L'Europe, Thethys II, Atalante and Pourquoi Pas, and the PIs M. Hamon, P. le Bot, C.

Accepted for publication in *Journal of Atmospheric and Oceanic Technology.* DOI 10.1175/JTECH-D-24-0009.1.

Kermabon, P.-M. Sarradin, M. Matabos, J. Sarrazin and J. Legrand. We also thank Ilker Fer from the University of Bergen who lent us a MicroRider-1000 for the first tests at the early stage of the project. The MicroRiYo project was funded by: the French Government, the European Fund for Economic and Regional Development, the Regional council of Brittany, and authorities of Finistère as part of the CPER project O3DO (2016-2020), the Interdisciplinary graduate school for the blue planet (ANR-17-EURE-0015, ISblue) and co-funded by a grant from the French government under the program "Investissements d'Avenir" embedded in France 2030 (Grants TUSIG and MicroRiYo@Sea). The deep VMP 6000 microstructure profilers were funded by the French Agence Nationale de la Recherche (ANR grant ANR-JC05_50690) and by the French Institute for Marine Science (IFREMER). The authors would also like to thank the two reviewers whose constructive comments have allowed us to improve the presentation of this study.

Data Availability Statement. Dissipation rate profiles, CTD and LADCP profiles from the MomarSat 2022 cruise are publicly available for non-commercial purpose at the SEANOE data archives: https://doi.org/10.17882/98361, https://doi.org/10.17882/94681.

REFERENCES

Budéus, G., K. Ohm, M. Damm, and R. Plugge, 2005: The externally powered, compressibility compensated Jojo mooring: A mechanical solution to autonomous deep sea profiling. *Deep-Sea Res. I*, **52**, 1964–1973, https://doi.org/10.1016/j.dsr.2005.05.005

Fer, I., A. K. Peterson, and J. E. Ullgren, 2014: Microstructure Measurements from an Underwater Glider in the Turbulent Faroe Bank Channel Overflow. *J. Atmos. Oceanic Technol.*, **31**, 1128–1150, https://doi.org/10.1175/JTECH-D-13-00221.1.

Ferron, B., P. B. Aubertot, Y. Cuypers, and C. Vic, 2023: Removing Biases in Oceanic Turbulent Kinetic Energy Dissipation Rate Estimated from Microstructure Shear Data. *J. Atmos. Oceanic Technol.*, **40**, 129–139, https://doi.org/10.1175/JTECH-D-22-0035.1.

Accepted for publication in *Journal of Atmospheric and Oceanic Technology.* DOI 10.1175/JTECH-D-24-0009.1.

Goodman, L., E. Levine, and R. Lueck, 2006: On measuring the terms of the turbulent kinetic energy budget from an AUV. J. Atmos. Oceanic Technol., 23, 977–990, https://doi.org/10. 1175/JTECH1889.1.

de Lavergne, C., G. Madec, J. Le Sommer, A. J. G. Nurser, and A. C. Naveira Garabato, 2016: On the Consumption of Antarctic Bottom Water in the Abyssal Ocean. *J. Phys. Oceanogr.*, **46**, 635–661, https://doi.org/10.1175/JPO-D-14-0201.1

de Lavergne, C., Vic, C., Madec, G., Roquet, F., Waterhouse, A. F., Whalen, C. B., et al., 2020: A parameterization of local and remote tidal mixing. Journal of Advances in Modeling Earth Systems, 12, e2020MS002065, https://doi.org/10.1029/2020MS002065

Lueck, R. G., 2022: The Statistics of Oceanic Turbulence Measurements. Part II: Shear Spectra and a New Spectral Model. J. Atmos. Oceanic Technol., 39, 1273–1282, https://doi.org/10.1175/JTECH-D-21-0050.1.

Polzin, K. L., and T. J. McDougall, 2022: Mixing at the ocean's bottom boundary. In M. P. Meredith & A. C. Naveira Garabato (Eds.), Ocean mix (pp. 145–180). Elsevier. https://doi.org/10.1016/b978-0-12-821512-8.00014-1

Prandke, H., K. Holtsch and A. Stips, 2000: MITEC technology development: The microstructure/turbulence measuring system MSS. Tech. Rep. EUR19733EN, Space Application Institute, Joint Research Centre European Commission, Ispra, Italy, 64 pp.

Wolk, F., H. Yamazaki, L. Seuront, and R. G. Lueck, 2002: A New Free-Fall Profiler for Measuring Biophysical Microstructure. *J. Atmos. Oceanic Technol.*, **19**, 780–793, https://doi.org/10.1175/1520-0426(2002)019<0780:ANFFPF>2.0.CO;2.

Accepted for publication in *Journal of Atmospheric and Oceanic Technology.* DOI 10.1175/JTECH-D-24-0009.1.